ACS APPLIED MATERIALS & INTERFACES

Research Article

www.acsami.org

Exploring the Effect of Band Alignment and Surface States on Photoinduced Electron Transfer from $CuInS_2$/CdS Core/Shell Quantum Dots to TiO_2 Electrodes

Mingye Sun,[†,‡] Dehua Zhu,[§] Wenyu Ji,[†] Pengtao Jing,[†] Xiuying Wang,[†] Weidong Xiang,*[,∥] and Jialong Zhao*[,†,§]

[†]State Key Laboratory of Luminescence and Applications, Changchun Institute of Optics, Fine Mechanics and Physics, Chinese Academy of Sciences, Changchun 130033, China

[‡]University of Chinese Academy of Sciences, Beijing 100039, China

[§]College of Mechanical and Electrical Engineering, Wenzhou University, Wenzhou 325035, China

[∥]College of Chemistry and Materials Engineering, Wenzhou University, Wenzhou 325035, China

Supporting Information

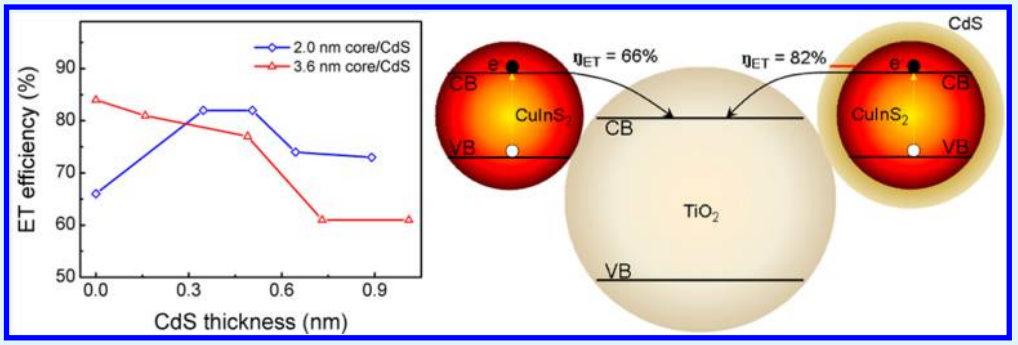

ABSTRACT: Photoinduced electron transfer (ET) processes from $CuInS_2$/CdS core/shell quantum dots (QDs) with different core sizes and shell thicknesses to TiO_2 electrodes were investigated by time-resolved photoluminescence (PL) spectroscopy. The ET rates and efficiencies from $CuInS_2$/CdS QDs to TiO_2 were superior to those of $CuInS_2$/ZnS QDs. An enhanced ET efficiency was surprisingly observed for 2.0 nm $CuInS_2$ core QDs after growth of the CdS shell. On the basis of the experimental and theoretical analysis, the improved performances of $CuInS_2$/CdS QDs were attributed to the passivation of nonradiative traps by overcoating shell and enhanced delocalization of electron wave function from core to CdS shell due to lower conduction band offset. These results indicated that the electron distribution regulated by the band alignment between core and shell of QDs and the passivation of surface defect states could improve ET performance between donor and acceptor.

KEYWORDS: *$CuInS_2$ quantum dots, TiO_2, electron transfer, band alignment, defect states*

1. INTRODUCTION

Great interests have been focused on quantum dot sensitized solar cells (QDSCs) in recent years due to the global energy crisis.[1] Unique features of quantum dots (QDs) such as size-tunable band gap,[2,3] high extinction coefficient,[4] and the multiple exciton generation[5] have made them good candidates for the design of the next-generation photovoltaics.[6−11] However, the maximum power conversion efficiency is typically below 5.5% for liquid junction QDSCs[12−15] and 5−7% for solid-state QDSCs,[16,17] which is influenced by the generation efficiency of electron−hole pairs, charge transfer dynamics, and electron recombination processes in these devices.[18]

Ternary chalcopyrite $CuInS_2$ is one kind of ideal semiconductor materials for designing and fabricating QDSCs due to its high absorption coefficient and direct bandgap of 1.5 eV which matches well with the solar spectrum.[19−22] Earlier $CuInS_2$-based liquid junction QDSCs showed a power conversion efficiency of less than 1%.[23] The efficiency of $CuInS_2$-based QDSCs was increased to 3.91% with the suppression of charge recombination at the TiO_2/QD/electrolyte interfaces by introducing a buffer layer and a passivation layer.[24−26] The Teng group made a great breakthrough in the $CuInS_2$-based solar cells by introducing a CdS passivation layer and achieved a power conversion efficiency of 4.2%.[27] Moreover, the introduction of a broad bandgap ZnS passivation layer could also improve the performance of QDSCs by preventing the electron trapping into surface states of QDs.[28] Because the trap states at interface/surface of QDs play an important role in degrading the performance of QDSCs, the effective passivation is

Received: September 16, 2013
Accepted: November 9, 2013
Published: November 9, 2013

necessary to reduce these negative effects.[18,27,28] In addition, by exchanging CdS with a Mn−CdS shell, the power conversion efficiency of $CuInS_2$−Mn−CdS QDSCs was boosted from 4.69% to 5.38%, resulting from improved interfacial charge transfer properties controlled by type II bandgap engineering in $CuInS_2$−Mn−CdS systems.[29] The assembled CdS/CdSe QD-sensitized photovoltaics exhibited a conversion efficiency of 5.32% for efficient extraction of photogenerated electrons and enhanced electron injection rate owing to inverted type-I energy level alignment between CdS core and CdSe shell.[13] Consequently, band alignment engineering significantly influences the solar energy conversion efficiency of QDSCs, which could be regulated by selecting appropriate semiconductor materials and varying the core size and shell thickness.

Theoretically, utilizing the excess photo energy to create additional electron-hole pairs (multiple exciton generation) can increase the thermodynamic energy conversion efficiency of single junction QDSCs to 44%.[5,18] Although huge numbers of researches were conducted to study the work mechanisms of photovoltaics and further improve device performance by optimizing device structure and material parameters, the actual energy conversion efficiency was far below the theoretical value.[12−17] Thus, more significant efforts should be made to change the present situation. The charge separation at the QD−metal oxide interface is a primary photophysical event leading to photocurrent generation in QDSCs. Efficient interface electron transfer (ET) from QDs to external electrodes is a crucial factor to further improve the power conversion efficiency of QDSCs.[30] A fair amount of works have been done to search approaches to promote ET between QDs and metal oxide nanoparticles or organic electron acceptors.[30−34] Kamat group studied the effects of the QD size and donor−acceptor distance on ET dynamic processes from CdSe QDs to TiO_2, ZnO, and SnO_2 nanoparticles.[30−32] Further the Lian group observed the effects of the ZnS shell thickness and band alignment between core and shell on the charge separation from type I CdSe/ZnS and type II CdTe/CdSe core/shell QDs to adsorbed organic electron acceptors.[33,34] But the photosensitizing properties of $CuInS_2$ QDs are less understood. So, it is necessary to study the extraction efficiency of photogenerated electrons from $CuInS_2$ QDs to external electrodes for improving the performance of QDSCs.

In this work, we investigated the ET from $CuInS_2$/CdS and $CuInS_2$/ZnS core/shell QDs to TiO_2 films by time-resolved photoluminescence (PL) spectroscopy. The band alignment in $CuInS_2$ core QDs could be regulated by CdS and ZnS shell materials, which can adjust the spatial distributions of the conduction band electron and valence band hole wave functions. More efficient ET was observed in $CuInS_2$/CdS−TiO_2 than that in $CuInS_2$/ZnS−TiO_2 and even $CuInS_2$−TiO_2 due to the effective passivation of surface defect states and enhanced electron wave function delocalization from the core to shell of QDs.

2. EXPERIMENTAL SECTION

2.1. Chemicals. Indium acetate ($In(OAc)_3$, 99.99%), cadmium oxide (CdO, 99.99%), zinc stearate ($ZnSt_2$, 12.5−14% ZnO), 1-octadecene (ODE, 90%), oleic acid (OA, 90%), 1-dodecanethiol (DDT, 98%), and 3-mercaptopropionic acid (MPA, 99%) were purchased from Alfa Aesar. Copper(I) iodide (CuI, 98%), sulfur powder (S, 99%), and trioctylphosphine (TOP, 99%) were purchased from Aldrich. TiO_2 powder (P25, a mixed phase of 80% anatase and 20% rutile; average size 25 nm) was purchased from Degussa.

2.2. Synthesis of $CuInS_2$/CdS and $CuInS_2$/ZnS Core/Shell QDs. $CuInS_2$ QDs were synthesized with a typical method reported previously.[35] A 95 mg portion of CuI (0.5 mmol), 146 mg of $In(OAc)_3$ (0.5 mmol), and 5 mL of DDT were loaded in a 25 mL of three-necked flask. The reaction mixture was degassed for 10 min under vacuum filled with argon three times and heated to 130 °C for about 10 min until a clear solution was formed. Then, the temperature was raised to 230 °C and maintained at that temperature for 5−40 min for differently sized $CuInS_2$ QDs. In the shell overcoating procedure, the cadmium precursor was prepared by a mixture of 258.4 mg of CdO, 2 mL of oleic acid, and 4 mL of ODE was heated to 180 °C in a 25 mL three-neck flask under argon until the solution turned to clear, and then, an additional 7.5 mL of ODE was injected to make the concentration of $Cd(OA)_2$ 0.15 mmol/mL. The growth of a CdS (ZnS) shell was also conducted as reported in the paper.[35] A mixture of 2 mmol of $Cd(OA)_2$ ($ZnSt_2$), 2 mmol of sulfur dissolved in 2 mL of trioctylphosphine, and 8 mL of ODE was added dropwise into the reaction solution at 210 °C, and an aliquot was taken from the reaction for different reaction time to obtain QDs with a series of shell thicknesses. All the reaction mixtures were diluted with toluene, methanol was added and then centrifuged to remove excess ligands and precursors. After repeating the process three times, the precipitated QD samples were dispensed in toluene for further experiments and measurements.

2.3. Fabrication of TiO_2 and QDs/TiO_2 Electrodes. The TiO_2 and SiO_2 pastes used in this work were fabricated by the same method reported before.[36] TiO_2 used above was P25 powders with average size of 25 nm purchased from Degussa. SiO_2 nanocrystals with average size of 20 nm were synthetized with a method previously reported.[37] A 0.45 mL portion of deionized water and 270.5 mg of ammonium hydroxide were added into 7.5 mL of ethanol with stirring. And this solution was injected into the mixed solution of 3.472 g of tetraethyl orthosilicate and 7.5 mL of ethanol with constant stirring for 5 days. The SiO_2 nanocrystals were precipitated with hexane and further isolated by centrifugation and decantation. TiO_2 and SiO_2 films were spread on glass by spin-coating their pastes onto glass substrates with a speed of 2000 rpm for 60 s, and the obtained electrodes were subsequently calcined at 500 °C in air for 60 min and then cooled to room temperature naturally. For the QDs-sensitization, the TiO_2 and SiO_2 electrodes were heated to ∼200 °C and immersed rapidly in an acetonitrile solution of MPA (1 M) and sulfuric acid (0.1 M) for 12 h and then rinsed thoroughly with acetonitrile and toluene. After that, the MPA-coated metallic oxide films were immersed in QDs in toluene for 12 h and then rinsed thoroughly with toluene.[32]

2.4. Characterization and Measurements. The absorption spectra of the colloidal QDs in toluene solution were recorded on a UV-3101PC UV-Vis-NIR scanning spectrophotometer (Shimadzu). Fluorescence spectra were recorded by a Hitachi F-7000 spectrophotometer. The sizes of QDs were measured by a Philips TECNAI G2 transmission electron microscope (TEM) operated at an accelerating voltage of 200 kV. TEM samples were prepared by drop-casting QDs dispersed in toluene onto carbon-coated 200 mesh copper TEM grids. Energy-dispersive X-ray spectroscopy (EDX) was measured for the elemental analysis of the QDs by using GENESIS 2000 XMS 60S scanning electron microscope equipped with a field emission gun and operated at 10 kV. X-ray diffraction (XRD) patterns were collected on a Rigaku XRD spectrometer. The time-resolved PL spectra were measured by LifeSpec-II dedicated lifetime spectrometer (Edinburgh Instruments). The excitation source was picosecond pulsed diode laser with a laser wavelength of 485 nm. All measurements were carried out at room temperature.

3. RESULTS AND DISCUSSION

The absorption and normalized PL spectra of $CuInS_2$ core and $CuInS_2$/CdS core/shell QDs are shown in Figure 1. The diameters of two $CuInS_2$ core QDs were determined to be 2.0 and 3.6 nm, respectively, as seen from the TEM images shown in Figure 2a and b. The TEM images of $CuInS_2$/CdS core/shell QDs are also shown in Figure 2c and d. The shell thicknesses

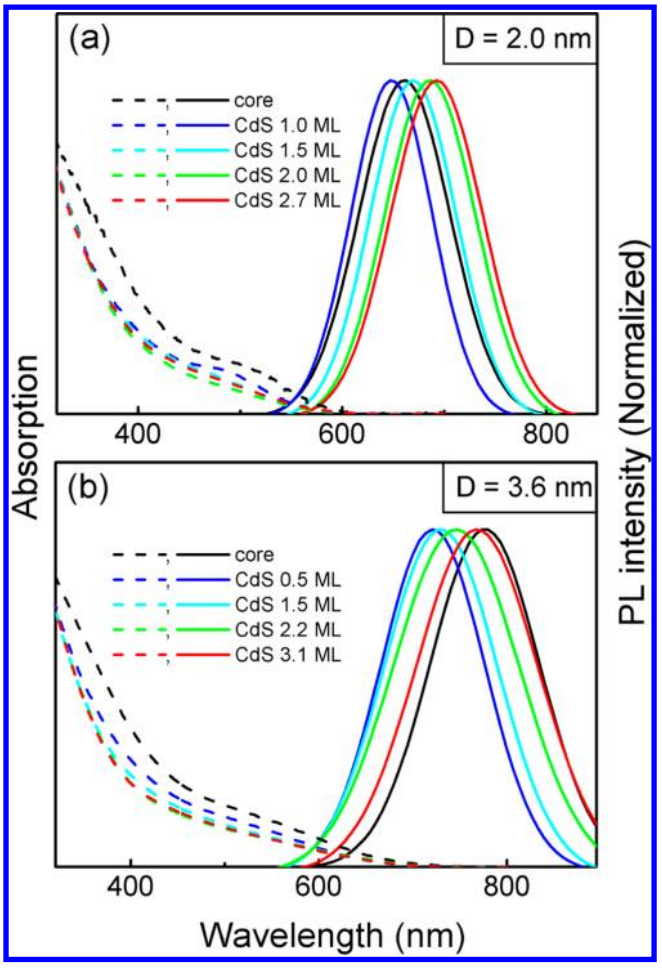

Figure 1. UV-visible absorption (dashed lines) and normalized PL (solid lines) spectra of 2.0 (a) and 3.6 nm (b) $CuInS_2$ core and $CuInS_2$/CdS core/shell QDs.

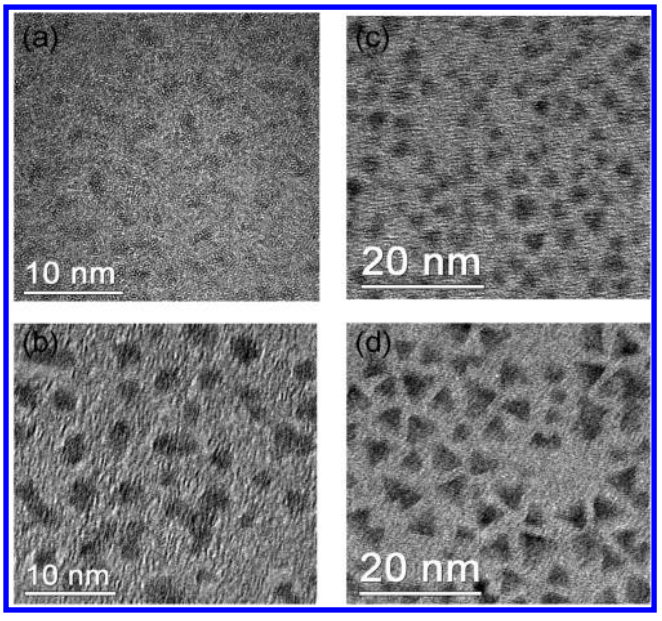

Figure 2. TEM images of bare $CuInS_2$ cores with 2.0 (a) and 3.6 nm (b) diameters and the corresponding $CuInS_2$/CdS core/shell QDs (c and d).

were approximately calculated by ignoring the size change of the $CuInS_2$ cores, and the shell layers were estimated on the basis of one monolayer (ML) of 0.31 and 0.33 nm with respect to ZnS and CdS shell materials. The corresponding TEM images and size distribution results of $CuInS_2$/CdS core/shell QDs with different core sizes and shell thicknesses are shown in Figures S1 and S2 in the Supporting Information. The XRD patterns of $CuInS_2$/CdS and $CuInS_2$/ZnS core/shell QDs were collected, and the composition of $CuInS_2$/CdS core/shell QDs with 2.0 nm core and 1.0 ML CdS shell was estimated by the EDX as shown in Supporting Information Figure S4. The Cu:In ratio is close to the ideal 1:1, and the XRD patterns are similar to those reported before,[35] ensuring the quality of the synthesized nanoparticles. As seen in Figures 1 and S5 (Supporting Information), the PL peaks of $CuInS_2$/CdS core/shell QDs exhibit a blue shift from 662 and 773 to 646 and 720 nm, respectively, relative to those of above-mentioned two $CuInS_2$ core QDs due to the etching of core and enhanced quantum confinement effect with the overgrowth of CdS shell, which is similar to ZnS overgrowth case. After that, further CdS shell overcoating produces a red shift from 646 and 720 to 692 and 765 nm, respectively, owing to delocalization of the electron wave function into CdS shell for a very small offset between the bulk conduction bands of the $CuInS_2$ core and CdS shell, as reported by the Klimov group.[35] It is worth noting that the PL peak of $CuInS_2$/CdS core/shell QDs with 2.7 ML shell shows a red shift of 30 nm relative to the corresponding bare QDs with 2.0 nm diameter. In contrary, the PL peak still exhibits a blue shift relative to pure $CuInS_2$ core QDs even though 3.1 ML CdS is overcoated for the 3.6 nm diameter $CuInS_2$ core QDs. These results suggest that the electron wave function delocalization from core to shell could be regulated not only by shell materials but (at least partly) by core sizes.

To acquire a deep understanding of the core size and shell material dependent distinctive performances, we measured the PL decays and estimated the average PL lifetimes of $CuInS_2$/CdS and $CuInS_2$/ZnS core/shell QDs with different core sizes and shell thicknesses as shown in Figure 3. The PL lifetimes of

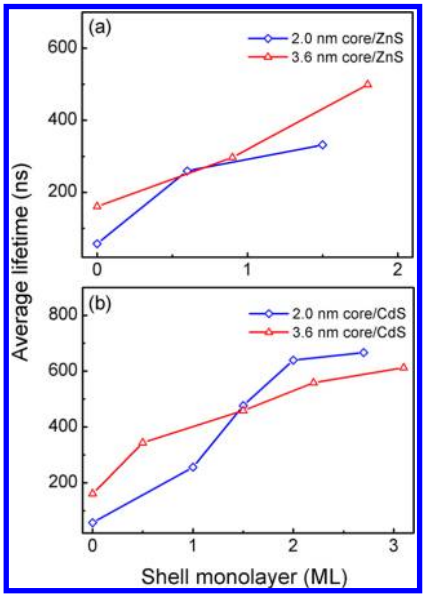

Figure 3. Average PL lifetimes of $CuInS_2$/ZnS (a) and $CuInS_2$/CdS (b) core/shell QDs with 2.0 (blue squares) and 3.6 nm (red triangles) core diameters and different shell thicknesses in toluene.

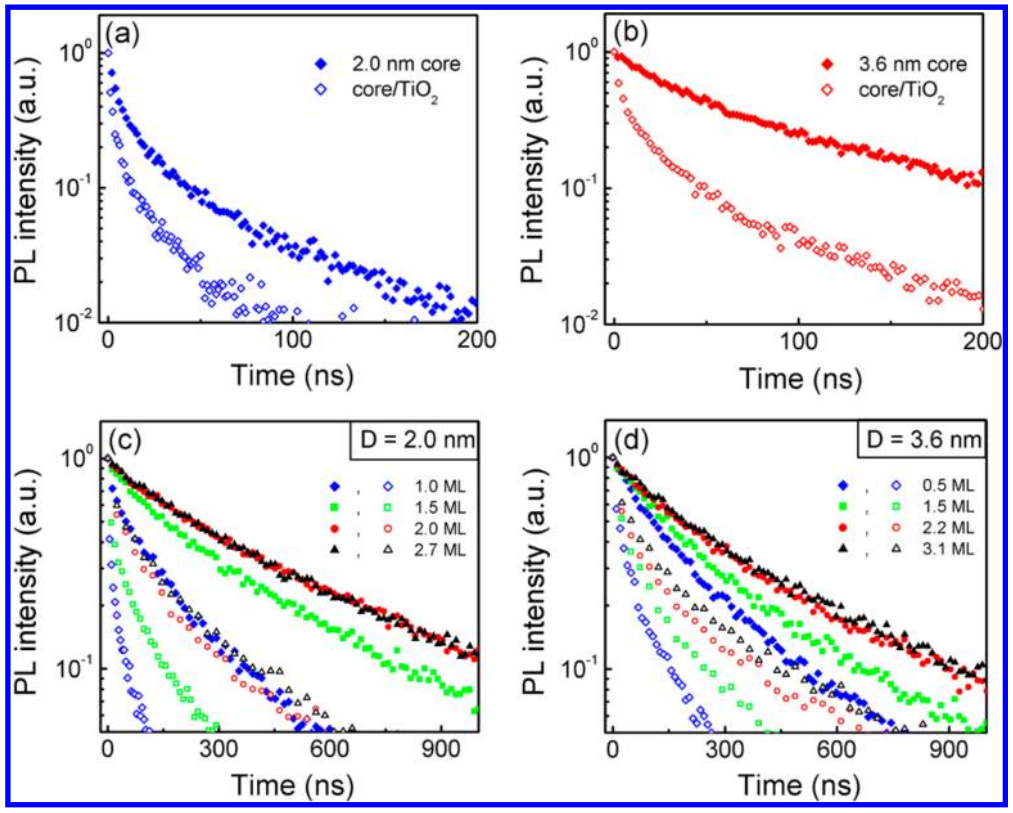

Figure 4. PL decay curves of 2.0 (a) and 3.6 nm (b) $CuInS_2$ core QDs and the corresponding $CuInS_2$/CdS core/shell QDs with 2.0 (c) and 3.6 nm (d) core diameters and various CdS shell thicknesses deposited on the TiO_2 (empty symbols) and SiO_2 (solid symbols) films.

$CuInS_2$ core QDs are shortened with decreasing the diameter and become long with increasing the shell thickness, indicating the effective passivation of surface states. Then, we measured the quantum yields and estimated the radiative and nonradiative decay rates of $CuInS_2$/CdS core/shell QDs using the relation $QY = k_r/(k_r + k_{nr})$ and $1/\tau = k_r + k_{nr}$ as listed in Table S1 in the Supporting Information. As seen from this table, the quantum yields increase and the nonradiative decay rates decrease from 1.66×10^7 and 5.52×10^6 s^{-1} for two $CuInS_2$ core QDs to 5.75×10^5 and 2.55×10^5 s^{-1} with the overgrowth of CdS shell, also confirming the effective passivation of nonradiative trap states by CdS shell. On the other hand, a surprising phenomenon is found that the average lifetimes of $CuInS_2$/ZnS core/shell QDs with a large core diameter are much longer than those of small core diameter QDs with similar ZnS shell thickness (Figure 3a),[38] but it turns to the opposite as to $CuInS_2$/CdS core/shell QDs (Figure 3b). This phenomenon can be understood as follows: lower offset between the bulk conduction bands of the $CuInS_2$ core and CdS shell relative to ZnS shell enhances the delocalization of electron wave function into shell. Meanwhile, the higher conduction band edge in the smaller $CuInS_2$ core relative to the larger one due to quantum confinement effect leads to a greater degree of delocalized electron wave function to CdS shell while the hole still remains in the $CuInS_2$ core, reducing the spatial overlap of photogenerated electron and hole wave functions inducing the slow radiative decay.[35] As shown in Supporting Information Table S1, the radiative decay rates of $CuInS_2$/CdS QDs with 2.0 nm core are obviously slower than those of QDs with 3.6 nm core. As discussed above, the spatial distribution of electron wave function could be tuned by adjusting the core sizes and shell materials (CdS, ZnS) to vary the band alignment between the core and shell. Therefore the enhanced electron wave function delocalization to CdS shell and shell-induced stability can make $CuInS_2$/CdS core/shell QDs a candidate for the fabrication of QDSCs.

The PL dynamics of $CuInS_2$/CdS core/shell QDs with different core sizes and shell thicknesses attached to TiO_2 and SiO_2 films were investigated and the corresponding PL decay curves are shown in Figure 4. It was feasible for ET from $CuInS_2$ core and $CuInS_2$/ZnS core/shell QDs to TiO_2 as observed in previous reports.[26,38] The SiO_2 is an insulator and it can not act as an electron acceptor. As seen in Figure 4c and d, the overcoating of CdS shell results in a significant increase in PL lifetimes and uniform single-exponential decays. After attaching $CuInS_2$/CdS core/shell QDs to TiO_2, a significant shortening in the PL decays is clearly observed as shown in Figure 4c and d. The ET rate (k_{ET}) and efficiency (η_{ET}) can be calculated from eqs 1 and 2:

$$k_{ET} = 1/\tau_{ave}(QD - TiO_2) - 1/\tau_{ave}(QD - SiO_2) \quad (1)$$

$$\eta_{ET} = 1 - \tau_{ave}(QD - TiO_2)/\tau_{ave}(QD - SiO_2) \quad (2)$$

where $\tau_{ave}(QD - TiO_2)$ and $\tau_{ave}(QD - SiO_2)$ are the average lifetimes of the QDs attached to TiO_2 and SiO_2 films, respectively. The ET rates and efficiencies were determined from eqs 1 and 2 and summarized in Table S2 in the Supporting Information. As seen from this table, the CdS shell layer has a significant influence on the ET from attached $CuInS_2$/CdS core/shell QDs to TiO_2. The ET rate decreases with the increase of CdS shell thickness for the role of shell as a tunneling barrier. Sun et al. found that the electrons had to tunnel through the shell barrier and transfer to TiO_2 in $CuInS_2$/ZnS-TiO_2 system, and the ET rates were in reasonable

agreement with the theoretical values of radial electron densities at the ZnS shell surfaces as a function of ZnS shell thickness in the following empirical formula:[38]

$$k_{ET}(d) = k_0 e^{-\beta d} \quad (3)$$

where d is the thickness of the shell and k_0 is the ET rate for bare QDs.[33] To quantify the effect of shell materials on the ET rate, the eigenfunctions and energies of the electrons in $CuInS_2$/CdS and $CuInS_2$/ZnS core/shell QDs were calculated by modeling them as particles confined in the spherical well of finite depth.[39,40] The effective mass of electrons is 0.16, 0.20, and $0.28m_0$ in $CuInS_2$,[41] CdS, and ZnS,[40] respectively. A potential energy of zero inside the $CuInS_2$ core and a barrier height of 0.05[26] and 1 eV[38] for electron to tunnel into CdS and ZnS shells are assigned. Another 3.7 eV barrier is assigned for electron to tunnel through to extend into the surrounding organic matrix (MPA).[38] The logarithm plots of ET rates and electron densities at CdS shell surfaces as a function of shell thickness for $CuInS_2$/CdS core/shell QDs with 2.0 and 3.6 nm core diameters are shown in Figure 5. In addition, for comparison the theoretical values of radial electron densities at the shell surfaces of $CuInS_2$/ZnS core/shell QDs with different core diameters and shell thicknesses are also presented in Figure 5, in consideration of the good fit between ET rates and theoretical values in $CuInS_2$/ZnS−TiO_2 system.[38] It is obvious that the rate of ET from $CuInS_2$/CdS core/shell QDs to TiO_2 is evidently faster than that of $CuInS_2$/ZnS core/shell QDs with the same core size and shell thickness. Figure 6c and d shows the radial distribution functions of lowest energy conduction band electrons of $CuInS_2$/CdS and $CuInS_2$/ZnS core/shell QDs with 2.0 ML shell (CdS, ZnS). It is obvious that lower offset between the bulk conduction bands of the $CuInS_2$ core and CdS shell (Figure 6a) relative to ZnS shell (Figure 6b) enhances the electron wave function delocalization from core to shell and electron density at the CdS shell surface. The electronic coupling strength between electron donor and acceptor for the ET process is proportional to the 1S electron density at the shell surface.[34] So the enhanced electron wave function delocalization and electron density accelerate the ET process from $CuInS_2$/CdS core/shell QDs to TiO_2.

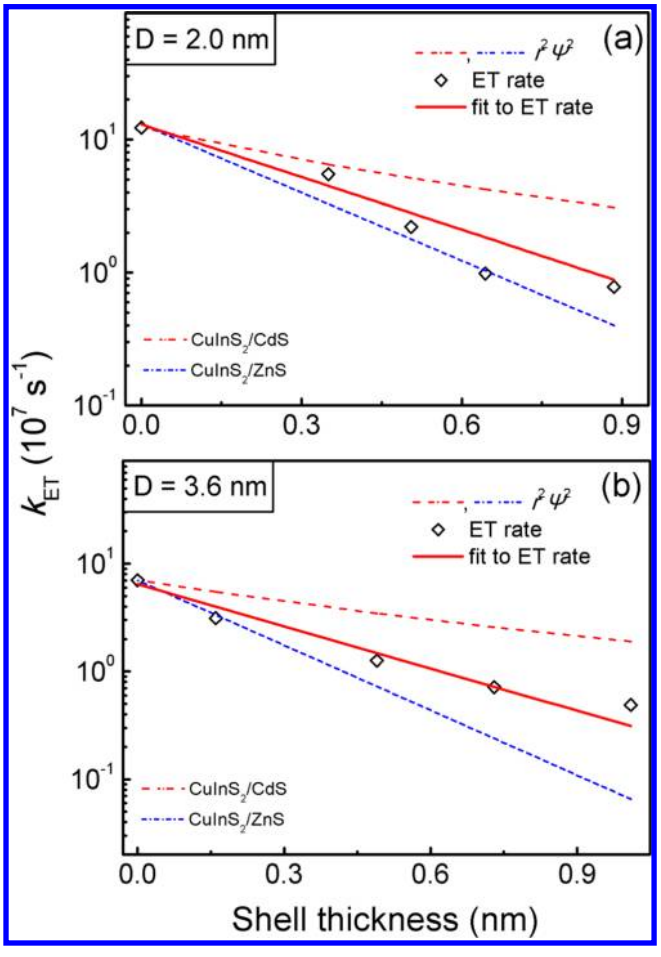

Figure 5. Plots of the logarithm of ET rates of $CuInS_2$/CdS core/shell QDs (black squares) with core diameters of 2.0 (a) and 3.6 nm (b) as a function of shell thickness. The solid lines represent the fit of the ET rates. The calculated electron densities at CdS (red dashed lines) and ZnS (blue short dash dot lines) shell surfaces as a function of shell thickness are also shown in the figure. The electron density lines are normalized to the measured ET rates of bare $CuInS_2$ QDs for comparison.

Nevertheless, the key issue for photovoltaics is not only the ET rate itself but also the ET efficiency generally. To investigate the improvement of ET efficiency in $CuInS_2$/CdS−TiO_2 and $CuInS_2$/ZnS−TiO_2 systems, the PL dynamics of $CuInS_2$/ZnS core/shell QDs with 2.0 and 3.6 nm core diameters and different shell thicknesses attached to TiO_2 films were investigated as described in Supporting Information Figure S6. The corresponding TEM images and size distribution results are shown in Supporting Information Figure S3. Meanwhile, the ET rates and efficiencies calculated are listed in Supporting Information Table S2. The experimental ET rates for $CuInS_2$/ZnS core/shell QDs are in reasonable agreement with the theoretical values, confirming the tunneling of the electron through the ZnS barrier shell.[38] The ET efficiencies for $CuInS_2$/CdS core/shell QDs are more efficient than those of $CuInS_2$/ZnS core/shell QDs with the same core diameter and similar shell thickness as shown in Table S2. And the advantage is more obvious when the shell gets thicker. This is because $CuInS_2$/ZnS core/shell QDs own a classic type I band alignment, and both the lowest energy conduction band electrons and valence band holes are confined in $CuInS_2$ core.[33] While, as to $CuInS_2$/CdS core/shell QDs, the initial intra-QD charge separation, enhanced electron wave function delocalization to CdS shell and increased electron density at the shell surface are in favor of ET from core/shell structure QDs to TiO_2.[34] The electron density at the QDs surface decreases exponentially with increasing the shell thickness in consideration of the tunneling of the electron through the barrier shell, so the advantage of $CuInS_2$/CdS core/shell QDs is highlighted compared to $CuInS_2$/ZnS core/shell QDs with increasing the shell thickness for lower offset between the bulk conduction bands of the $CuInS_2$ core and CdS shell relative to ZnS shell.

Moreover, the CdS shell-thickness-dependent ET efficiencies were explored as shown in Figure 7. The ET efficiency decreases from 84% for bare core to 81%, 77%, and 61% for 3.6 nm core QDs with 0.5, 1.5, and 3.1 ML CdS shell, respectively, but it increases surprisingly from 66% for 2.0 nm bare core to 82% and 73% for QDs with 1.0 and 2.7 ML CdS shell, respectively, as seen in Figure 7. While the ET efficiency decreased with the increase of shell thickness was reported from classic type I band alignment $CuInS_2$/ZnS and gradient CdSe/ZnS core/shell QDs to TiO_2 and ZnO films, respectively.[38,42] The surprising increase in ET efficiency for

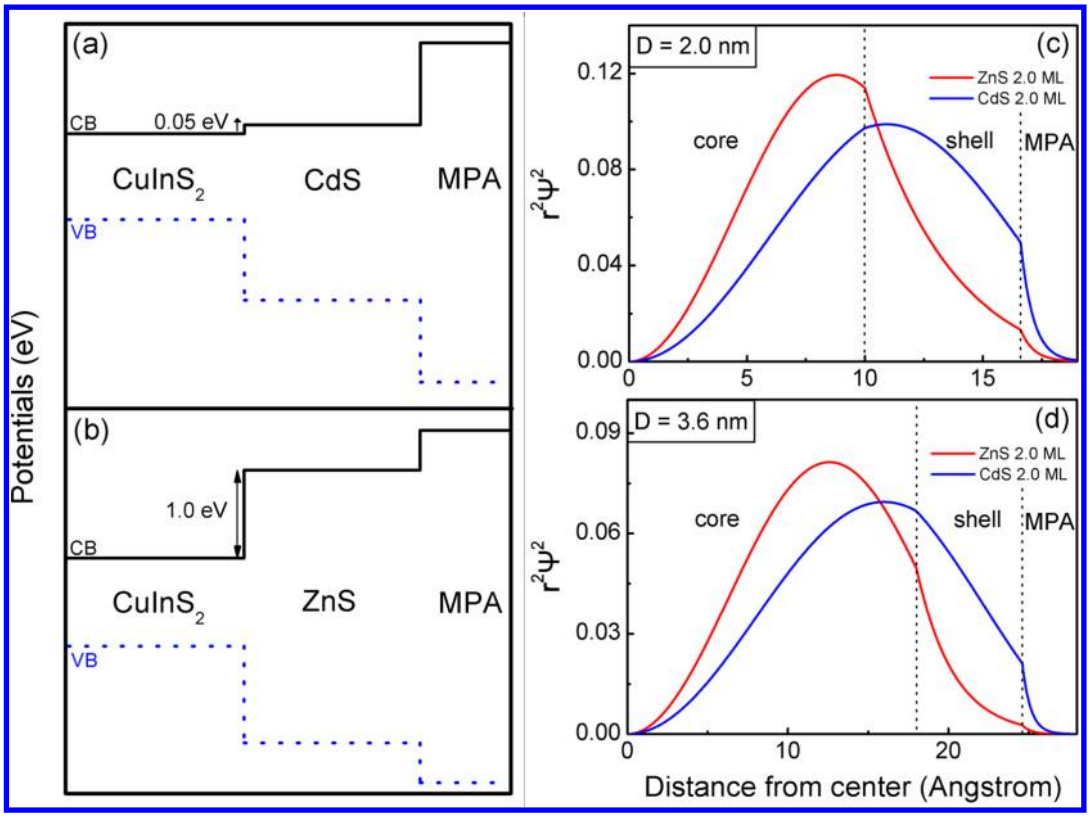

Figure 6. Schematic illustration of the band level alignment for $CuInS_2$/CdS (a) and $CuInS_2$/ZnS (b) core/shell QDs and the radial distribution functions of lowest energy conduction band electrons of $CuInS_2$/CdS (blue lines) and $CuInS_2$/ZnS (red lines) core/shell QDs with 2.0 (c) and 3.6 nm (d) core diameters and 2.0 ML shell.

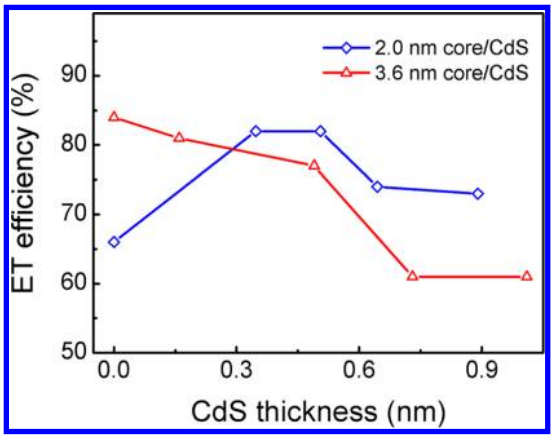

Figure 7. ET efficiencies of $CuInS_2$/CdS core/shell QDs with core diameters of 2.0 (blue squares) and 3.6 nm (red triangles) and different CdS shell thicknesses attached to TiO_2 films.

2.0 nm $CuInS_2$ QDs after overgrowth of the CdS shell found in our work can be explained below. The conduction band of bulk $CuInS_2$ is only 0.05 eV lower than that of bulk CdS, making the electron wave function delocalize to CdS shell easily as seen in Figure 6. The enhanced electron wave function delocalization is in favor of efficient ET for increased electronic coupling between $CuInS_2$/CdS core/shell QDs and TiO_2. While the delocalization of hole wave function from $CuInS_2$ core to shell is difficult due to high tunneling barrier induced by CdS shell.[33,34] So the spatial overlap of photogenerated electron and hole wave functions reduces after CdS shell overcoating, and this spatial distribution results in a fast and efficient ET.[34] Moreover, the exceedingly large surface-to-volume ratio and a high density of surface states of nanoparticles usually enhance the effect of surface on electron dynamics.[43] The surface passivation of the QDs by broad bandgap semiconductor shell overcoating (CdS, ZnS) could improve the ET process and then enhance the performance of QDSCs by suppressing the surface trapping.[27,28,44] The nonradiative decay rates of $CuInS_2$ QDs decrease rapidly after CdS shell overgrowth as shown in Supporting Information Table S1, indicating that CdS shell overgrowth around $CuInS_2$ bare QDs could passivate the traps as nonradiative recombination centers competing with ET.[18,45,46] This means that the passivation of nonradiative traps by overcoating shell, the enhanced electron wave function delocalization to shell, and reduced spatial overlap between electron and hole wave functions make the ET for $CuInS_2$/CdS core/shell QDs with 2.0 nm core diameter more efficient relative to bare core. But the ET efficiency for $CuInS_2$/CdS core/shell QDs with 3.6 nm core diameter shows a slight reduction for decreased electron wave function delocalization to shell due to increased potential barrier between core and shell with larger core size. It is worth mentioning that the ET efficiency still stays at a high level for CdS shell thickness up to ~1.5 MLs as shown in Figure 7. So about 1.0–2.0 ML CdS shell passivation around $CuInS_2$ QDs could not only make QDs more stable but also reduce the unwanted back-recombination of the injected electrons with little expense of ET efficiency in the design of QDSCs.

Then, we fit the theoretical electron densities and experimental ET rates of $CuInS_2$/CdS core/shell QDs with eq 3, the values of β are 1.68 and 3.03 nm^{-1} for the QDs with 2.0 nm core diameter and 1.38 and 3.01 nm^{-1} for QDs with

large core as shown in Figure 5a and b.[33,38] A gap between experimental ET rates and calculated radial electron densities at CdS shell surfaces is clearly seen for the same $CuInS_2$/CdS core/shell QDs. In addition, this confusing situation is not discovered for $CuInS_2$/ZnS core/shell QDs as seen in Supporting Information Figure S6c.[38] As what has been said above, the difference between experimental and theoretical values comes from the change of shell materials. The enhanced electron wave function delocalization from $CuInS_2$ core to CdS shell relative to much higher conduction band ZnS shell makes itself more sensitive to surface defects.[39,47] Meanwhile, the QD surface defects as nonradiative recombination centers will compete efficiently with the ET and significantly influence the electron injection process.[18,45,46] So, the difference between experimental ET rates and calculated radial electron densities for $CuInS_2$/CdS core/shell QDs possibly arises from increased effect of QD surface defects on ET process. Further work is necessary to verify the exact mechanisms of $CuInS_2$ QD-based solar cells and optimize their performances.

4. CONCLUSIONS

In conclusion, we have demonstrated efficient ET from $CuInS_2$/CdS core/shell QDs with different core sizes and shell thicknesses to TiO_2 electrodes. An improvement in ET rate and efficiency is observed for $CuInS_2$/CdS QDs relative to $CuInS_2$/ZnS QDs with the same core size and shell thickness, due to initial intra-QD charge separation, enhanced electron wave function delocalization to CdS shell, and increased electron density at the shell surface for CdS shell QDs for lower conduction band offset. The ET efficiency increases from 66% for 2.0 nm bare core QDs to 82% after overgrowth of 1.0 ML CdS shell surprisingly, resulted from passivation of surface defects, enhanced electron wave function delocalization to shell and reduced spatial overlap between electron and hole wave functions. These results demonstrate the improved ET performance by passivating the surface states and tuning the band alignment between core and shell of QDs and suggest the rational design of QD-sensitizer with low conduction band edge passivation layer in QDSCs.

■ ASSOCIATED CONTENT

Supporting Information

Typical TEM images, size distributions, and PL peak positions of $CuInS_2$/CdS and $CuInS_2$/ZnS QDs. XRD patterns of $CuInS_2$/CdS and $CuInS_2$/ZnS QDs and EDX spectrum of $CuInS_2$/CdS QDs with 2.0 nm core and 1.0 ML CdS shell. PL decay curves of $CuInS_2$/ZnS QDs attached to TiO_2 and SiO_2 films and ET rates and efficiencies of $CuInS_2$/CdS and $CuInS_2$/ZnS QDs with different shell thicknesses. PL quantum yields, radiative and nonradiative decay rates of $CuInS_2$/CdS core/shell QDs. This material is available free of charge via the Internet at http://pubs.acs.org.

■ AUTHOR INFORMATION

Corresponding Authors

*Phone: +86 577 86689613. E-mail: xiangweidong001@126.com.

*Phone: +86 431 86176313. E-mail: zhaojl@ciomp.ac.cn.

Notes

The authors declare no competing financial interest.

■ ACKNOWLEDGMENTS

This work was supported by the National Natural Science Foundation of China (Nos. 11274304, 61205025, 51102227, and 11204298).

■ REFERENCES

(1) Barnham, K. W. J.; Mazzer, M.; Clive, B. *Nat. Mater.* **2006**, *5*, 161−164.
(2) Sarma, D. D.; Nag, A.; Santra, P. K.; Kumar, A.; Sapra, S.; Mahadevan, P. *J. Phys. Chem. Lett.* **2010**, *1*, 2149−2153.
(3) Dohnalová, K.; Poddubny, A. N.; Prokofiev, A. A.; de Boer, W. D. A. M.; Umesh, C. P.; Paulusse, J. M. J.; Zuilhof, H.; Gregorkiewicz, T. *Light: Sci. Appl.* **2013**, *2*, e47.
(4) Yu, W. W.; Qu, L. H.; Guo, W. Z.; Peng, X. G. *Chem. Mater.* **2003**, *15*, 2854−2860.
(5) Beard, M. C. *J. Phys. Chem. Lett.* **2011**, *2*, 1282−1288.
(6) Kalyanasundaram, K.; Grätzel, M. *J. Mater. Chem.* **2012**, *22*, 24190−24194.
(7) Kamat, P. V.; Tvrdy, K.; Baker, D. R.; Radich, J. G. *Chem. Rev.* **2010**, *110*, 6664−6688.
(8) Nozik, A. J.; Beard, M. C.; Luther, J. M.; Law, M.; Ellingson, R. J.; Johnson, J. C. *Chem. Rev.* **2010**, *110*, 6873−6890.
(9) Selinsky, R. S.; Ding, Q.; Faber, M. S.; Wright, J. C.; Jin, S. *Chem. Soc. Rev.* **2013**, *42*, 2963−2985.
(10) Kramer, I. J.; Sargent, E. H. *ACS Nano* **2011**, *5*, 8506−8514.
(11) Tang, J.; Sargent, E. H. *Adv. Mater.* **2011**, *23*, 12−29.
(12) Santra, P. K.; Kamat, P. V. *J. Am. Chem. Soc.* **2012**, *134*, 2508−2511.
(13) Pan, Z. X.; Zhang, H.; Cheng, K.; Hou, Y. M.; Hua, J. L.; Zhong, X. H. *ACS Nano* **2012**, *6*, 3982−3991.
(14) Yu, X. Y.; Liao, J. Y.; Qiu, K. Q.; Kuang, D. B.; Su, C. Y. *ACS Nano* **2011**, *5*, 9494−9500.
(15) Radich, J. G.; Dwyer, R.; Kamat, P. V. *J. Phys. Chem. Lett.* **2011**, *2*, 2453−2460.
(16) Ip, A. H.; Thon, S. M.; Hoogland, S.; Voznyy, O.; Zhitomirsky, D.; Debnath, R.; Levina, L.; Rollny, L. R.; Carey, G. H.; Fischer, A.; et al. *Nat. Nanotechnol.* **2012**, *7*, 577−582.
(17) Chang, J. A.; Rhee, J. H.; Im, S. H.; Lee, Y. H.; Kim, H. J.; Seok, S. I.; Nazeeruddin, M. K.; Grätzel, M. *Nano Lett.* **2010**, *10*, 2609−2612.
(18) Yang, Z. S.; Chen, C. Y.; Roy, P.; Chang, H. T. *Chem. Commun.* **2011**, *47*, 9561−9571.
(19) Kruszynska, M.; Borchert, H.; Parisi, J.; Kolny-Olesiak, J. *J. Am. Chem. Soc.* **2010**, *132*, 15976−15986.
(20) Nairn, J. J.; Shapiro, P. J.; Twamley, B.; Pounds, T.; Wandruszka, R.; Fletcher, T. R.; Williams, M.; Wang, C. M.; Norton, M. G. *Nano Lett.* **2006**, *6*, 1218−1223.
(21) Cho, J. W.; Park, S. J.; Kim, J.; Kim, W.; Park, H. K.; Do, Y. R.; Min, B. K. *ACS Appl. Mater. Interfaces* **2012**, *4*, 849−853.
(22) Zhang, Z. Y.; Zhang, X. Y.; Xu, H. X.; Liu, Z. H.; Pang, S. P.; Zhou, X. H.; Dong, S. M.; Chen, X.; Cui, G. L. *ACS Appl. Mater. Interfaces* **2012**, *4*, 6242−6246.
(23) Kuo, K. T.; Liu, D. M.; Chen, S. Y.; Lin, C. C. *J. Mater. Chem.* **2009**, *19*, 6780−6788.
(24) Chang, J. Y.; Su, L. F.; Li, C. H.; Chang, C. C.; Lin, J. M. *Chem. Commun.* **2012**, *48*, 4848−4850.
(25) Xu, G. P.; Ji, S. L.; Miao, C. H.; Liu, G. D.; Ye, C. H. *J. Mater. Chem.* **2012**, *22*, 4890−4896.
(26) Santra, P. K.; Nair, P. V.; Thomas, K. G.; Kamat, P. V. *J. Phys. Chem. Lett.* **2013**, *4*, 722−729.
(27) Li, T. L.; Lee, Y. L.; Teng, H. *Energy Environ. Sci.* **2012**, *5*, 5315−5324.
(28) Guijarro, N.; Campiña, J. M.; Shen, Q.; Toyoda, T.; Lana-Villarreal, T.; Gómez, R. *Phys. Chem. Chem. Phys.* **2011**, *13*, 12024−12032.
(29) Luo, J. H.; Wei, H. Y.; Huang, Q. L.; Hu, X.; Zhao, H. F.; Yu, R. C.; Li, D. M.; Luo, Y. H.; Meng, Q. B. *Chem. Commun.* **2013**, *49*, 3881−3883.

(30) Kamat, P. V. *Acc. Chem. Res.* **2012**, *45*, 1906−1915.
(31) Robel, I.; Kuno, M.; Kamat, P. V. *J. Am. Chem. Soc.* **2007**, *129*, 4136−4137.
(32) Kongkanand, A.; Tvrdy, K.; Takechi, K.; Kuno, M.; Kamat, P. V. *J. Am. Chem. Soc.* **2008**, *130*, 4007−4015.
(33) Zhu, H. M.; Song, N. H.; Lian, T. Q. *J. Am. Chem. Soc.* **2010**, *132*, 15038−15045.
(34) Zhu, H. M.; Song, N. H.; Lian, T. Q. *J. Am. Chem. Soc.* **2011**, *133*, 8762−8771.
(35) Li, L.; Pandey, A.; Werder, D. J.; Khanal, B. P.; Pietryga, J. M.; Klimov, V. I. *J. Am. Chem. Soc.* **2011**, *133*, 1176−1179.
(36) Ito, S.; Chen, P.; Comte, P.; Nazeeruddin, M. K.; Liska, P.; Péchy, P.; Grätzel, M. *Prog. Photovolt: Res. Appl.* **2007**, *15*, 603−612.
(37) Stöber, W.; Fink, A.; Bohn, E. *J. Colloid Interface Sci.* **1968**, *26*, 62−69.
(38) Sun, J. H.; Zhao, J. L.; Masumoto, Y. *Appl. Phys. Lett.* **2013**, *102*, 053119.
(39) Dabbousi, B. O.; Rodriguez-Viejo, J.; Mikulec, F. V.; Heine, J. R.; Mattoussi, H.; Ober, R.; Jensen, K. F.; Bawendi, M. G. *J. Phys. Chem. B* **1997**, *101*, 9463−9475.
(40) Haus, J. W.; Zhou, H. S.; Honma, I.; Komiyama, H. *Phys. Rev. B* **1993**, *47*, 1359−1365.
(41) Zhong, H. Z.; Zhou, Y.; Ye, M. F.; He, Y. J.; Ye, J. P.; He, C.; Yang, C. H.; Li, Y. F. *Chem. Mater.* **2008**, *20*, 6434−6443.
(42) Abdellah, M.; Žídek, K.; Zheng, K. B.; Chábera, P.; Messing, M. E.; Pullerits, T. *J. Phys. Chem. Lett.* **2013**, *4*, 1760−1765.
(43) Zhang, J. Z. *Acc. Chem. Res.* **1997**, *30*, 423−429.
(44) Shen, Q.; Kobayashi, J.; Diguna, L. J.; Toyoda, T. *J. Appl. Phys.* **2008**, *103*, 084304.
(45) Hetsch, F.; Xu, X. Q.; Wang, H. K.; Kershaw, S. V.; Rogach, A. L. *J. Phys. Chem. Lett.* **2011**, *2*, 1879−1887.
(46) Cánovas, E.; Moll, P.; Jensen, S. A.; Gao, Y. N.; Houtepen, A. J.; Siebbeles, L. D. A.; Kinge, S.; Bonn, M. *Nano Lett.* **2011**, *11*, 5234−5239.
(47) Peng, X. G.; Schlamp, M. C.; Kadavanich, A. V.; Alivisatos, A. P. *J. Am. Chem. Soc.* **1997**, *119*, 7019−7029.